Density-functional theory calculations of optical rotatory dispersion in the nonresonant and resonant frequency regions

Patrick Norman[a)]
Department of Physics and Measurement Technology, Linköping University, SE-581 83 Linköping, Sweden

Kenneth Ruud
Department of Chemistry, University of Tromsø, N-9037 Tromsø, Norway

Trygve Helgaker
Department of Chemistry, University of Oslo, P.O. Box 1033 Blindern, N-0315 Oslo, Norway

(Received 1 December 2003; accepted 19 December 2003)

The complex linear response function, which can be employed for calculations of second-order molecular properties in regions of strong absorption, is here extended to encompass the mixed electric-dipole–magnetic-dipole polarizability. The mixed electric-dipole–magnetic-dipole polarizability determines the optical rotation and, when absorption is taken into account, the full anomalous optical rotatory dispersion (ORD) spectra of chiral molecules can be calculated using first-principle quantum-chemical methods. Gauge-origin independence of the results is ensured through the use of London atomic orbitals. To illustrate the importance of taking the absorption process properly into account, we here apply this methodology to the study of the anomalous ORD of hydrogen peroxide, 3R-methylcyclohexanone, 4R-1,1-dimethyl-[3]-(1,2)-ferrocenophan-2-on, and the D_2 isomer of the C_{84} fullerene. © *2004 American Institute of Physics.*
[DOI: 10.1063/1.1647515]

I. INTRODUCTION

From a historical perspective, optical rotatory dispersion (ORD) has been an important method for determining the energy and character of the excited states of chiral molecules.[1] In ORD measurements, the optical rotation of a chiral molecule is studied as a function of the frequency of the incident light. Assuming a sufficient separation of the excited electronic states, these states can often be determined as the frequencies at which the optical rotation vanishes (although we will return to exceptions to this later in this paper) in what is known as the anomalous ORD effect.[1] However, with the introduction of electronic circular dichroism, ORD lost much of its importance. Today, optical rotations are used mainly for determining the stereochemistry of a chiral molecule by measurements at a single frequency, usually that of the sodium D line.

Microscopically, the optical rotation of a molecule is determined by the trace of the mixed electric-dipole–magnetic-dipole polarizability $G'_{\alpha\beta}$,

$$G'_{\alpha\beta} = \mathrm{Im}\langle\langle \hat{\mu}_\alpha ; \hat{m}_\beta \rangle\rangle_\omega = -2\omega \sum_{n\neq 0} \mathrm{Im} \frac{\langle 0|\hat{\mu}_\alpha|n\rangle\langle n|\hat{m}_\beta|0\rangle}{(\omega_{n0}-\omega)^2}, \quad (1)$$

where $\hat{\mu}_\alpha$ and $\hat{m}_\beta$ are components of the electric and magnetic dipole operators, respectively, and ω is the frequency of the incident light. The kets $|0\rangle$ and $|n\rangle$ denote, respectively, the electronic ground state and the nth excited state of the molecule, $\hbar\omega_{n0}$ is the corresponding excitation energy from the ground state, and the summation includes all excited states. Note that this polarizability vanishes in the limit of static electromagnetic fields. Furthermore, the magnetic dipole operator has a dependence on a magnetic gauge origin, and it is only the trace of the mixed polarizability tensor that is origin independent. From the sum-over-states expression in Eq. (1), we note that the calculated mixed polarizability diverges as the frequency of the incident light approaches an excitation energy of the molecule ($\omega \rightarrow \omega_{n0}$).

In theoretical calculations of ORD, the following three computational issues must be addressed. First, the frequency-dependent mixed electric dipole–magnetic dipole polarizability must be calculated; second, the gauge-origin dependence of the magnetic dipole operator must be properly treated; third, the divergence of the mixed electric-dipole–magnetic-dipole polarizability in regions of strong absorption must be handled correctly.

The frequency-dependent mixed electric-dipole–magnetic-dipole polarizability can be calculated using analytic linear response theory,[2] as first demonstrated by Polavarapu[3] using an implementation of $G'_{\alpha\beta}$ developed for the calculation of vibrational Raman optical activity (VROA).[4] The analytical calculation of $G'_{\alpha\beta}$ was later extended to density-functional theory (DFT) by Stephens and co-workers.[5] Very recently, the first coupled-cluster calculations have been presented.[6,7] We note that, for the calculation of optical rotation, a static-field approximation can be used.[8] However, since such an approach does not give the correct frequency dependence, it is not suited to the study of ORD.

In approximate calculations, the magnetic dipole operator displays a dependence on the gauge origin different from that of the exact operator. The calculated optical rotation

[a)]Electronic mail: panor@ifm.liu.se

therefore depends on the choice of gauge origin; only in the limit of a complete basis set will variational methods give the correct origin dependence of the magnetic dipole operator. However, as demonstrated in Ref. 4, the use of London atomic orbitals[9] in conjunction with the natural connection[10] ensures that, for variational wave functions, the magnetic dipole operator has the correct dependence on the global gauge origin—even for finite basis sets. In this paper, London orbitals are used to ensure that our calculated ORDs are gauge-origin independent.

The third problem—that is, the divergence of the mixed electric-dipole–magnetic-dipole polarizability tensor—has so far not been dealt with in the literature. Polavarapu and Zhao presented a theoretical investigation of the ORD of different conformations of 3R-methylcyclohexanone at the Hartree–Fock level,[3] showing that the correct form of the Cotton curves can be obtained, but also clearly demonstrating the divergence of the method as the frequency of the incident light approaches that of the Hartree–Fock excitation energies. In addition to the problems with the divergences, the Hartree–Fock excitation energy was off by about 0.75 eV compared to experiment.[11,12]

In this paper, we aim to rectify the problem of divergences in the mixed electric-dipole–magnetic-dipole polarizability tensor through the use of complex response functions.[13] The basic ansatz in this approach is to introduce a finite lifetime for the excited states, thereby obtaining a physically correct description of the molecular response also in the resonant regions.

In Sec. II, we outline the calculation of ORD using complex response theory. Section III provides some details of the calculations we have carried out to illustrate the performance of our code; the results of these calculations are presented in Sec. IV. Finally, we give some concluding remarks in Sec. V.

II. THEORY AND METHODOLOGY

A. Natural optical rotation

In isotropic samples and in the absence of static fields, only chiral molecules display natural optical activity. The change in light polarization upon passage through the sample has a microscopic origin in the coupling between the electric field-induced polarization and the time-dependent magnetic field of the radiation. The natural optical rotation (rad/m) for a monochromatic light beam of frequency ω (rad) is given by[14]

$$\Delta\theta = -\tfrac{1}{3}\omega\mu_0 N G'_{\alpha\alpha}(\omega), \tag{2}$$

where N (m^{-3}) is the number density, μ_0 is the permeability of vacuum, and G' is the coupling tensor. An implied Einstein summation is assumed for repeated indices and applies here to the Cartesian axis α.

Let us consider a molecular perturbation that is spatially uniform and periodic. The electric and magnetic fields can then be written as

$$F_\alpha(t) = \sum_{k=-N}^{N} F_\alpha^{\omega_k} e^{-i\omega_k t}, \tag{3}$$

$$B_\alpha(t) = \sum_{k=-N}^{N} B_\alpha^{\omega_k} e^{-i\omega_k t}, \tag{4}$$

where $\omega_{-k} = -\omega_k$, $F^{-\omega_k} = F^{\omega_k *}$, and $B^{-\omega_k} = B^{\omega_k *}$. Furthermore, the static components are zero—that is, $F^{\omega_0} = B^{\omega_0} = 0$ for $\omega_0 = 0$. Including only the terms linear in fields, the molecular polarization in the presence of these perturbing fields is given by

$$\mu_\alpha(t) = \mu_\alpha^0 + \sum_{k=-N}^{N} [\alpha_{\alpha\beta}(\omega_k) F_\beta^{\omega_k} + \chi_{\alpha\beta}(\omega_k) B_\beta^{\omega_k}] e^{-i\omega_k t}, \tag{5}$$

where μ^0 is the permanent electric dipole moment, $\alpha(\omega)$ is the frequency-dependent electric dipole polarizability, and $\chi(\omega)$ is the linear coupling to the external magnetic field. The strength of the natural optical rotation $G'(\omega)$ as given by Barron[14] corresponds to

$$G'(\omega) = \frac{1}{2i}[\chi(\omega) - \chi(-\omega)], \tag{6}$$

where $\chi(-\omega) = \chi(\omega)^*$.

B. Sum-over-states expression

A quantum mechanical expression for the optical rotatory dispersion parameter $\chi(\omega)$ is obtained from perturbation theory. We need to consider the response of the wave function to the magnetic field only. Alternatively, we may determine the correction to the molecular magnetic dipole moment due to the time-dependent electric field $F_\alpha(t)$ and make use of the fact that the linear response function is unchanged with respect to interchanging pairs of operators and associated frequencies. The time-development of the system is governed by the Schrödinger equation

$$i\hbar \frac{\partial}{\partial t} |\psi(t)\rangle = H|\psi(t)\rangle, \tag{7}$$

where the Hamiltonian H can be divided into the unperturbed molecular Hamiltonian H_0 and the perturbation $V(t)$. The ground state is assumed to be of singlet spin symmetry and the only coupling with the external magnetic field is provided by the orbital angular-momentum operator. The perturbation is then given by

$$V(t) = -\hat{m}_\alpha B_\alpha(t) = -\frac{1}{2}\sum_{i=1}^{N_e} l_{i,\alpha}^O B_\alpha(t), \tag{8}$$

where N_e is the number of electrons in the system, $\hat{m}$ is the electronic magnetic moment operator, and l_i^O is the orbital angular-momentum operator for electron i with respect to the origin O. Before the perturbation is switched on, the system is assumed to be in its ground state $|0\rangle$. The subsequent time-evolution can be parametrized as

$$|\psi(t)\rangle = e^{-\hat{P}(t)}|0\rangle, \tag{9}$$

where $\hat{P}$ is an anti-Hermitian operator of the form

$$\hat{P}(t) = \sum_{n>0} [P_n|n\rangle\langle 0| - P_n^*|0\rangle\langle n|]. \tag{10}$$

The state transfer operators $\hat{\Omega}_n=|n\rangle\langle 0|$ and $\hat{\Omega}_n^\dagger=|0\rangle\langle n|$ connect the ground state and the residual set of eigenstates to H_0. The set of time-dependent amplitudes $\{P_n,P_n^*\}$ are found from the equation-of-motion

$$\frac{\partial}{\partial t}\langle\psi(t)|\hat{\Omega}_n|\psi(t)\rangle=\frac{1}{i\hbar}\langle\psi(t)|[\hat{\Omega}_n,H]|\psi(t)\rangle - \gamma_n[\langle\psi(t)|\hat{\Omega}_n|\psi(t)\rangle-\langle 0|\hat{\Omega}_n|0\rangle]. \tag{11}$$

A second set of equations is obtained by applying Eq. (11) to $\hat{\Omega}_n^\dagger$. This equation is recognized as the Ehrenfest theorem with an additional term that introduces depopulation of the excited states through the damping factor γ. Using the density operator $\hat{\rho}(t)=|\psi(t)\rangle\langle\psi(t)|$, this equation can be recast in the form of the Liouville equation. The infinite-lifetime approximation, which is often adopted, corresponds to $\gamma=0$.

The set of amplitudes are expanded to various order in the perturbation

$$P_n=P_n^{(1)}+P_n^{(2)}+P_n^{(3)}+\cdots, \tag{12}$$

and the Baker–Campbell–Hausdorff (BCH) expansion is invoked in Eq. (11) after inserting Eq. (9). The first-order amplitudes are retrieved from the resulting equation, which is linear in $\hat{P}$ and the perturbation $V(t)$:

$$\frac{\partial}{\partial t}\langle 0|[\hat{P},\hat{\Omega}_n]|0\rangle=\frac{1}{i\hbar}[\langle 0|[\hat{P},[\hat{\Omega}_n,H_0]]|0\rangle + \langle 0|[\hat{\Omega}_n,V(t)]|0\rangle] - \gamma_n\langle 0|[\hat{P},\hat{\Omega}_n]|0\rangle. \tag{13}$$

The solution of this equation for $P_n^{(1)}$ gives us

$$P_n^{(1)}=\frac{1}{\hbar}\sum_{k=-N}^{N}\frac{\langle n|\hat{m}_\alpha|0\rangle B_\alpha^{\omega_k}e^{-i\omega_k t}}{-\omega_{n0}+\omega_k+i\gamma_n}, \tag{14}$$

where we have introduced the excitation energy $\hbar\omega_{n0}=E_n-E_0$. By considering the corresponding first-order correction to the wave function

$$|\psi^{(1)}\rangle=-\sum_{n>0}P_n^{(1)}|n\rangle, \tag{15}$$

we arrive at the first-order magnetic-field induced molecular polarization

$$\langle 0|\hat{\mu}_\alpha|\psi^{(1)}\rangle+\langle\psi^{(1)}|\hat{\mu}_\alpha|0\rangle = \sum_{k=-N}^{N}\frac{1}{\hbar}\sum_{n>0}\left[\frac{\langle 0|\hat{\mu}_\alpha|n\rangle\langle n|\hat{m}_\beta|0\rangle B_\beta^{\omega_k}}{\omega_{n0}-\omega_k-i\gamma_n}e^{-i\omega_k t} + \frac{\langle n|\hat{m}_\beta|0\rangle^*\langle n|\hat{\mu}_\alpha|0\rangle B_\beta^{-\omega_k}}{\omega_{n0}-\omega_k+i\gamma_n}e^{i\omega_k t}\right]. \tag{16}$$

If we make use of the fact that the summation runs over both positive and negative frequencies so that ω_k can be replaced by $-\omega_k$ in the second term, then a straightforward identification with Eq. (5) gives

$$\chi_{\alpha\beta}(\omega_k)=\frac{1}{\hbar}\sum_{n>0}\left[\frac{\langle 0|\hat{\mu}_\alpha|n\rangle\langle n|\hat{m}_\beta|0\rangle}{\omega_{n0}-\omega_k-i\gamma_n} + \frac{\langle 0|\hat{m}_\beta|n\rangle\langle n|\hat{\mu}_\alpha|0\rangle}{\omega_{n0}+\omega_k+i\gamma_n}\right]. \tag{17}$$

C. Approximate state theory

In practice, we want to evaluate Eq. (17) without explicit knowledge of the eigenstates of H_0. The electric and magnetic dipole transition matrix elements can be obtained in approximate state theories and, at least in principle, the summation in Eq. (17) can be evaluated. Such an approach suffers from slow convergence and is seldom used in conjuction with standard *ab initio* electronic structure methods. A much better alternative is to formulate the approximate polarization propagator—see, for instance, the work by Olsen and Jørgensen.[2] The linear polarization propagator has been extended to encompass absorption in the system by Norman *et al.*,[13] no longer relying on the infinite-lifetime approximation. Moreover, near-resonant electric-field induced polarizations can be addressed.[13] In the present work, this technique is used for magnetic-field induced polarizations.

We consider the case of a single-determinant reference state as assumed in closed-shell Hartree–Fock and Kohn–Sham theories. The reference state can then be parametrized as

$$|\psi(t)\rangle=e^{-\hat{\kappa}}|0\rangle, \tag{18}$$

where the initial state $|0\rangle$ is a Slater determinant of orthonormalized molecular orbitals. The anti-Hermitian operator $\hat{\kappa}$ can be written as

$$\hat{\kappa}=\sum_a\sum_i[\kappa_{si}a_s^\dagger a_i-\kappa_{si}^*a_i^\dagger a_s], \tag{19}$$

where s and i denote unoccupied and doubly occupied molecular orbitals, respectively, and $a_s^\dagger a_i$ is a pair of creation and annihilation operators. The time-dependence of the parameters κ_{si} can be determined by applying the Ehrenfest theorem with damping [cf. Eq. (11)] to the orbital transfer operators $\hat{q}_{si}^\dagger=a_s^\dagger a_i$ and $\hat{q}_{si}=a_i^\dagger a_s$. The resulting equation-of-motion for the amplitudes holds to each order in the perturbation as well as at each optical frequency. In the implementation,[13] we used a common lifetime broadening factor γ for all excited states. An order in the perturbation expansion is introduced for the amplitudes

$$\kappa_{si}=\kappa_{si}^{(1)}+\kappa_{si}^{(2)}+\kappa_{si}^{(3)}+\cdots, \tag{20}$$

and the first-order solution to the equation-of-motion is found by introducing the frequency decomposition of the amplitudes

$$\kappa_{si}^{(1)}(t)=\sum_{k=-N}^{N}\kappa_{si}^{(1)}(\omega_k)e^{-i\omega_k t}, \tag{21}$$

$$\kappa_{si}^{(1)*}(t) = \sum_{k=-N}^{N} \kappa_{si}^{(1)*}(\omega_k) e^{i\omega_k t}$$

$$= \sum_{k=-N}^{N} \kappa_{si}^{(1)*}(-\omega_k) e^{-i\omega_k t}. \quad (22)$$

The first-order response is given by

$$\begin{bmatrix} \kappa^{(1)}(\omega_k) \\ \kappa^{(1)*}(-\omega_k) \end{bmatrix} = (E^{[2]} - \hbar(\omega_k + i\gamma)S^{[2]})^{-1} \times \begin{bmatrix} \langle 0|[-\hat{q}^\dagger, \hat{m}_\alpha]|0\rangle \\ \langle 0|[\hat{q}, \hat{m}_\alpha]|0\rangle \end{bmatrix} B_\alpha^{\omega_k}, \quad (23)$$

where the amplitudes and the perturbation have been collected in column vectors. The dimension of this matrix equation is equal to twice the number of paired indices (s,i). Since the elements of the $S^{[2]}$ matrix are the overlaps between the singly excited determinants, $S^{[2]}$ is diagonal. The $E^{[2]}$ matrix, also known as the Hessian matrix, collects the contributions from the unperturbed Hamiltonian H_0.

With the first-order corrections at hand, we can collect the first-order contribution to the molecular polarization, which arises from the term $\langle 0|[\hat{\kappa}, \hat{\mu}_\alpha]|0\rangle$ in the BCH expansion of the expectation value of the electric dipole operator. Written as a vector product, we thus obtain a first-order magnetic-field induced polarization as

$$\chi_{\alpha\beta}(\omega_k) = \begin{bmatrix} \langle 0|[\hat{q}, \hat{\mu}_\alpha]|0\rangle \\ \langle 0|[-\hat{q}^\dagger, \hat{\mu}_\alpha]|0\rangle \end{bmatrix}^\dagger (E^{[2]} - \hbar(\omega_k + i\gamma)S^{[2]})^{-1} \times \begin{bmatrix} \langle 0|[-\hat{q}^\dagger, \hat{m}_\beta]|0\rangle \\ \langle 0|[\hat{q}, \hat{m}_\beta]|0\rangle \end{bmatrix}. \quad (24)$$

The implementation of Eq. (24) has been described in Ref. 13. The introduction of the lifetime broadening factor γ couples the real and imaginary parts of $\chi(\omega)$ and gives a physically correct propagator, also in the near-resonant and resonant regions of the spectrum.

We have so far not discussed the evaluation of the magnetic property gradient in Eq. (24) which, because of the orbital angular-momentum operator, carries a dependence on the choice of gauge origin. This problem has been considered and resolved by Helgaker *et al.* in their work on VROA.[4] The same magnetic property gradients are used here.

III. COMPUTATIONAL DETAILS

The calculations in the present work have been performed using a single-determinant parametrization of the reference states, adopting the time-dependent Hartree–Fock (TDHF) and the time-dependent Kohn–Sham (TDKS) approximations. In the TDKS calculations, we employ the B3LYP[15] exchange–correlation functional for geometry optimizations as well as for the molecular property calculations.

For hydrogen peroxide, the geometries are those of Ref. 16. All other structures have been optimized at the DFT/B3LYP level. Due to the varying size of the systems, we have employed different basis sets in these geometry optimizations; the cc-pVDZ basis[17,18] is used for the structure optimization of 3R-methylcyclohexanone and the 6-31G basis set[19] for the fullerene C_{84}. The B3LYP optimized structure for ferrocene is that obtained by Grimme *et al.*,[20] which was kindly provided to us.[21] As depicted in Fig. 1, 3R-methylcyclohexanone has been optimized in its 3S forms. However, to comply with the work of Polavarapu and Zhao,[3] the Cotton curves have been presented for the corresponding 3R forms—that is, with a mere change of sign.

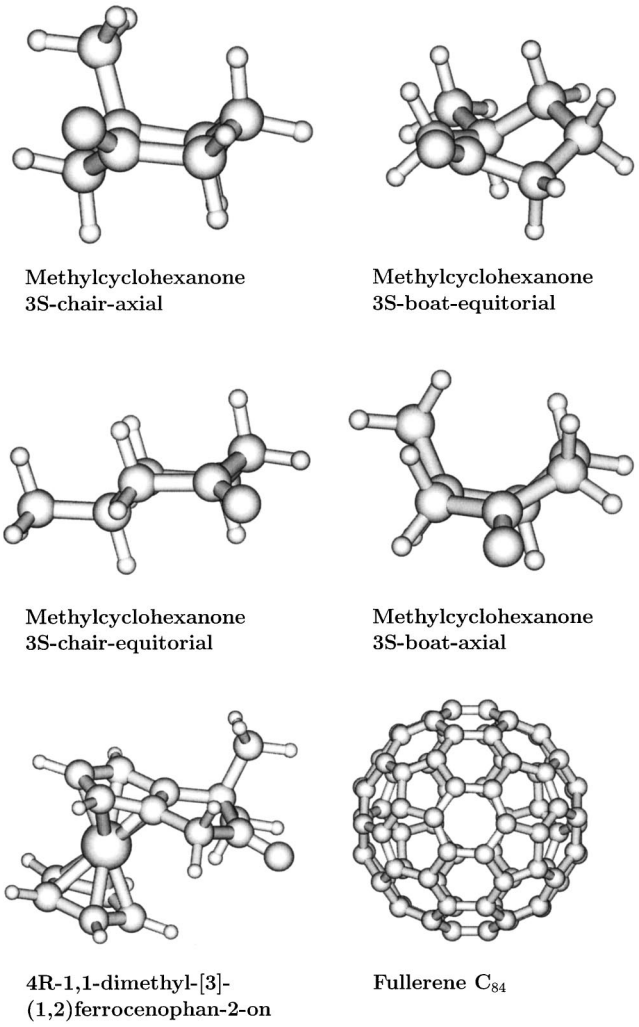

FIG. 1. Molecular structures.

The property calculations have been performed using the polarization propagator approach, often referred to as the TDHF and TDKS approximations. The derivation of the linear response function was outlined in Sec. II; a detailed description of the implementation of the complex linear polarization propagator is found in Ref. 13. A lifetime-broadening value of $\gamma = 1000\ \mathrm{cm}^{-1}$ was used in all ORD calculations. The basis sets used in the calculations of excitation energies and optical rotatory dispersions are the daug-cc-pVTZ basis[17,18] for hydrogen peroxide, the aug-cc-pVDZ basis[17,18] for 3R-methylcyclohexanone and the 6-31G basis[19] for C_{84}. For ferrocene, we used the cc-pVDZ basis[17] for the light elements and a split-valence triple-zeta basis[22] for iron.

With the exception of the geometry optimization of C_{84}, which was carried with the GAUSSIAN 98 program,[23] all cal-

culations reported have been performed with a locally modified version of the DALTON program.[24]

IV. RESULTS AND DISCUSSION

A. Anomalous dispersion

Let us first point out that the notion of anomalous dispersion is neither more nor less connected with ORD than with any other second-order molecular property described by a response function such as that in Eq. (17). Examples of properties with the same dispersion are the electric and magnetic dipole polarizabilities, as is easily seen from the pole structure of the response functions. When implementing Eq. (17) in the infinite-lifetime approximation—that is, with $\gamma_n = 0$—one must maintain a reasonable detuning in the calculation to obtain a physically correct result. It is also possible to perform calculations beyond the first resonance energy, but it becomes increasingly more difficult to apply this approach due the large density of states at short wavelengths. Results for ORD in the short-wavelength region between the first and second excited states have been presented in the literature.[3]

B. Damping term

The damping terms in our implementation corresponds to the inverse lifetime of the excited states. It is well known that the lifetime of the singlet states in organic molecules varies quite strongly—typically, the first excited state is longer-lived than states that are higher in energy. When the system is no longer isolated, it may undergo collisions with other molecules—for example, in gas phase or in solution—which may alter the phase of the wave functions in an unpredictable manner.[25] Effectively, this complicated process may be treated in a statistical sense with the damping (or, equivalently, the lifetime broadening) terms. Values in the order of 0.1 eV or about $800\ \mathrm{cm}^{-1}$ have been used in a similar context in semi-empirical calculations—see, for instance, Ref. 26. In the propagator theory used in the present work, the lifetime broadening term is also semi-empirical in nature.

Since it is mainly governed by intermolecular interactions, it is difficult to determine the value of γ by means of first-principle calculations and no such attempt is made here. In the original presentation of the implementation of the complex response function, the effect of varying γ was investigated.[13] A smaller value of γ causes the absorption band to become narrower but also more intense. In the present work, we have used the value of $\gamma = 1000\ \mathrm{cm}^{-1}$, keeping in mind that it must be carefully tuned against the experiment to have predictive power. We will therefore *not* draw any conclusions in the present work that depend critically on the choice of this parameter.

C. Hydrogen peroxide

The optical rotation of hydrogen peroxide as a function of the dihedral angle has received much theoretical interest recently.[6,16] In spite of its simple molecular structure, theoretical studies at a wavelength of 589 nm have found the optical rotation to vary by more than $400°/(\mathrm{dm\,g/cm^3})$ as the dihedral angle changes.[6,16] Also, the optical rotation accidentally becomes zero even when the molecule is chiral. In the case of H_2O_2 and H_2S_2,[16,27] the vanishing of the optical rotation for one chiral configuration is mainly due to the accidental degeneracy of the two lowest excited states, which are of opposite polarizations. Clearly, it is of some interest to consider the ORD of H_2O_2 both for dihedral angles close to this accidental degeneracy and for angles where the two lowest excited states are energetically separated.

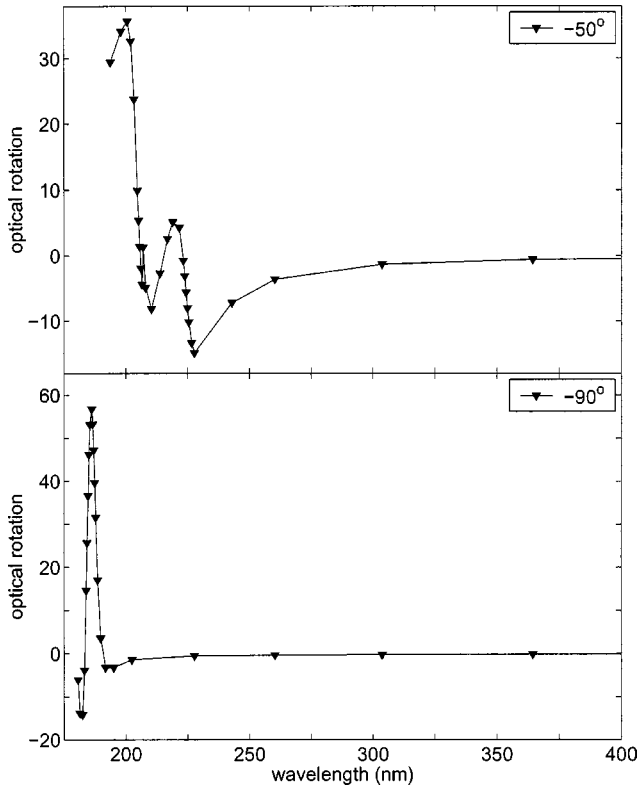

FIG. 2. Optical rotatory dispersion curves for hydrogen peroxide for dihedral angles of $-50°$ (top) and $-90°$ (bottom). The ORD is given in $10^3°/(\mathrm{dm\,g/cm^3})$ and the wavelength in nm.

In Fig. 2, we show the ORD curves for the hydrogen peroxide molecule at dihedral angles of $-50°$ and $-90°$. Whereas the former angle corresponds to the configuration with the largest negative optical rotation at the sodium *D* line,[6,16] the latter is close to where the two lowest-lying excited states become degenerate. The difference between the two curves is striking. Clearly, ORD is capable of providing detailed information about the structure of molecular excited states.

At a dihedral angle of $-50°$, the calculated excitation energies for the two lowest states are 5.53 and 6.03 eV, respectively, corresponding to excitation wavelengths of 224 and 206 nm. Both excitation energies are easy to locate as points where the optical rotation changes from negative to positive, see Fig. 2. However, we also note that the optical rotation passes through zero at about 215 nm, even though there is no excited state at this energy. The reason for this perhaps surprising result can be understood from the sum-over-states expression in Eq. (1). We first recall that, in the

slightly different case of the electric polarizability, the numerator is always positive for the diagonal tensor elements, and the sign of the polarizability is therefore determined solely by the energy spectrum. In contrast, for the mixed electric-dipole–magnetic-dipole polarizability, the diagonal elements of G' have different signs,[28] leading to cancellations when taking the trace in Eq. (2). Since the different elements in the trace may show different dispersion characteristics, dispersion alone (without passing through an excitation) may lead to zero optical rotation as observed in Fig. 2 at about 215 nm and at the dihedral angle of $-50°$.

The change in the sign of the numerator in the sum-over-states expression [Eq. (1)] is important not only in absorptive regions, where the dispersion is strong. Indeed, the same effect also occurs for a dihedral angle of 100°, where the optical rotations at 589 and 456 nm are -6 and $+5°/(\mathrm{dm\,g/cm^3})$, respectively, with both wavelengths well separated from the lowest excitation wavelength of 191 nm. This sign change of the numerator in the optical rotation tensor is also part of the reason for the change in sign of the optical rotation observed when comparing gas-phase and liquid-phase experiments for methyloxirane.[29,30]

Turning our attention to the ORD of H_2O_2 at a dihedral angle of $-90°$, we note that the two lowest excited states are nearly degenerate, the excitation energies being 6.63 and 6.71 eV at the B3LYP level. This near-denegeracy leads to a very narrow Cotton effect (within the limitations of our approach). Interestingly, the third and fourth lowest excited states also become almost degenerate (and close to the two lowest excited states), the calculated excitation energies being 6.89 and 6.92 eV, respectively.

D. 3R-methylcyclohexanone

Having considered the model system H_2O_2, we now turn our attention to a system for which earlier experimental and theoretical data have been presented. The ORD of 3R-methylcyclohexanone (3MCH) in the chair and boat conformations and with an equatorial placement of the methyl group has been studied theoretically by Polavarapu and Zhao.[3] Their results have been compared with the corresponding experimental spectra[11,12] for the (+)-enantiomer—that is, the 3R-chair-equatorial form, which includes the resonant region of optical frequencies.

A shortcoming of the theoretical treatment of Polavarapu and Zhao is the use of an uncorrelated electronic-structure method, i.e., the Hartree–Fock method, in combination with the infinite-lifetime approximation in the propagator calculation. The use of the Hartree–Fock method for this organic molecule inflicts a well-known overestimation of the excitation energy. Thus, the Hartree–Fock transition wavelength is 252 nm,[3] which corresponds to an error in the transition energy of 0.75 eV relative to the experimentally observed wavelength of 297 nm,[11,12] making it impossible to perform accurate calculations of the ORD in the resonance region since the dispersion is largely determined by the excitation energies of the system. In Fig. 3, the TDHF and TDKS/B3LYP excitation energies are included as vertical lines; the former is virtually identical to the literature value of 252 nm,[3] whereas the correlated DFT/B3LYP result is in perfect

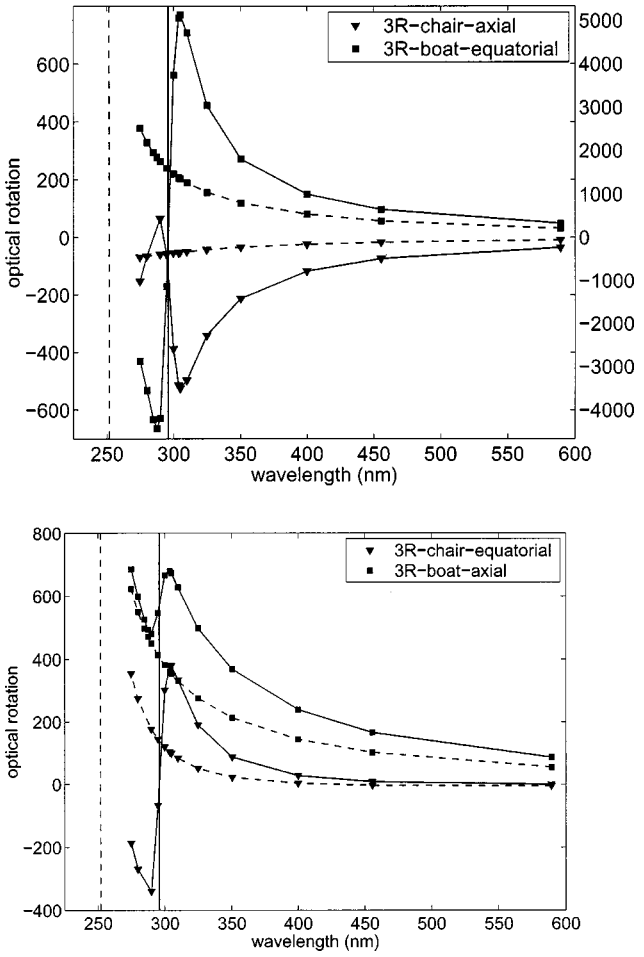

FIG. 3. Optical rotatory dispersion curves for the axial and equitorial form of 3-methylcyclohexanone. The left and right scales in the upper figure refers to the 3R-chair-axial and 3R-boat-equitorial forms, respectively. The vertical lines mark the lowest singlet transition wavelengths. Results are obtained with TDHF (dashed lines) and TDKS/B3LYP (solid lines). The ORD is given in degrees/$(\mathrm{dm\,g/cm^3})$ and the wavelength in nm.

agreement with the experimental value of 297 nm. It appears that we have an accurate description of the ground and first excited states, and that we should be in a good position to calculate the ORD down to about 290 nm. In Fig. 3, it is seen that there are sizable differences between the TDHF and TDKS predictions of the ORD also in the region of no absorption. Since optical rotations are usually predicted with much better reliability using TDKS/B3LYP than TDHF,[31] it can be assumed that our TDKS calculation is the better estimate in the whole frequency region.

At the respective optimized geometries, the DFT/B3LYP total energy of 3MCH in the 3R-chair-equatorial form is 1.58 kcal/mol lower than that of the 3R-chair-axial form. Since the two boat forms are significantly higher in energy, the theoretical results for these conformations are likely to be of lesser interest to experimentalists. Their ORD spectra are included here for sake of completeness.

Comparing with the results of Polavarapu and Zhao presented in Fig. 1 of Ref. 3, the most striking difference relative to our results in Fig. 3 is the absence of divergences. The use of a complex propagator theory enables us not only to determine the positive (3R-chair-equatorial) and negative

TABLE I. Excitation energies for low-lying states of singlet spin symmetry in 4R-1,1-dimethyl-[3]-(1,2)ferrocenophan-2-on.

	$1\,^1A$		$2\,^1A$	
	(eV)	(nm)	(eV)	(nm)
TDHF	0.675	1837	0.714	1735
TDKS/B3LYP	2.395	518	2.398	517

TABLE II. Optical rotation [deg/[dm g/cm^3]] at wavelengths λ (nm) for 4R-1,1-dimethyl-[3]-(1,2)ferrocenophan-2-on.

λ	TDHF	TDKS/B3LYP
1059.6	−9.1	11.4
694.6	−13.3	24.4
624.2	−15.6	28.7
589.3	···	30.7
579.7	···	31.2

(3R-chair-axial) Cotton curves for the two chair conformations, but also to determine the widths of the ORD, which are found to be about 15 nm for the chair conformations. As discussed earlier, the amplitude of the ORD is largely determined by the chosen lifetime of the excited states and cannot be directly compared with experiment. However, if the reliability of the complex response theory calculations of ORD can be benchmarked, the combination of experimental anomalous ORD spectra and calculated ORD spectra may provide a viable approach to determine the lifetime of singlet excited electronic states.

In Fig. 3, we have also included results for 3MCH in the boat forms. While there is no noticeable difference in the excitation energies for any of the four conformations, the Cotton effect is qualitatively different in the chair and the boat conformations. The boat conformations both show a positive Cotton effect, whereas the sign differs in the two cases for the axial ones. The amplitude of the ORD for the 3R-boat-equatorial form of 3MCH is also significantly larger than for any of the other conformations. Since the experimental spectrum shows a clear positive Cotton curve,[11,12] it is clear that the solution contained a surplus of the chair-equatorial conformation, which is also in agreement with it being lower in energy.

E. Ferrocene

In a recent study, Grimme *et al.*[20] calculated the optical rotation for eight molecules at the TDKS level using two different exchange–correlation functionals. With the exception of 4R-1,1-dimethyl-[3]-(1,2)-ferrocenophan-2-on, the B3LYP results were in fair agreement with the experimental results.[20] For this particular ferrocene derivative, on the other hand, the value at the sodium *D* line was calculated to be positive, whereas the experiment shows a negative Cotton effect. The authors point out that this is a difficult system to treat theoretically since the sodium *D* line falls inside the first absorption band with a maximum around 600 nm, and that calculations of circular dichroism spectra are to be preferred.[20] From the previous discussion, it is clear that caution is called for with respect to calculations at a single frequency because of the anomalous dispersion in the vicinity of an absorption band, but that the dispersion can be addressed theoretically with inclusion of damping terms in the propagator.

Ferrocene itself possesses a C_5 rotational symmetry axis with a resulting doubly degenerate first excited state arising from iron *d*-electron excitations. From symmetry arguments, this degeneracy is lifted in the derivate; in practice, the lowest excited states in the derivative are virtually the same as in ferrocene itself. In Table I, we present the theoretical estimates of the lowest excited singlet states. The Hartree–Fock model fails miserably to describe the excitation in this transition metal complex—the excitation energies for the two lowest states are predicted to be 0.675 and 0.714 eV, or about 1700–1800 nm, which is energetically far below the experimentally observed λ_{max} of about 600 nm.[20] This situation is rectified with the use of DFT, and, at the B3LYP level, the two lowest states are nearly degenerate, in accordance with our discussion above. The transition wavelengths reported here are in the region 517–518 nm, overestimating the excitation energy relative to experiment.

From Table II, we see that the TDHF Cotton curve is indeed negative, in agreement with the experiment. However, in light of the above-noted discussion on excitation energies, the uncorrelated ORD values are not meaningful. By contrast, the B3LYP optical rotation is positive at frequencies below the first transition frequency. It would therefore be of interest to obtain an experimental result at a wavelength longer than λ_{max}. In the spectra presented for 3MCH above, it was seen that the dispersion is very strong in the vicinity of the resonance and that a transition from positive to negative ORD values may occur within a few nanometers. In view of the virtues of DFT for ORD calculations, we believe that the Cotton curve is indeed positive in the limit of long wavelengths, and that the experimental value recorded at 589.3 nm is negative because of a sign change around λ_{max}. Although the B3LYP exchange–correlation functional does not fully reproduce the correct transition energy, the main features of the spectrum are most likely correct.

F. Fullerene C_{84}

A number of isomers of the fullerene C_{84} are known, the most abundant being the D_2 and D_{2d} isomers. Some of the isomers have been obtained in purified forms and comparisons between experimental spectra and quantum chemical calculations are used for assignments.[32] The electron spin resonance spectrum of the D_2 isomer shows a strong temperature dependence, interpreted as a thermal population of low-lying excited spin states.[32] The calculations reported in this work are to be compared with the zero-temperature limit of the isolated species and also ignore zero-point vibrational motions.[28]

Linear absorption spectra, theoretical and experimental, are reported mainly for the smaller fullerenes since isomer separation is an issue for fullerenes beginning with C_{78}. A detailed comparison between TDKS and experimental results has been made for C_{60}, C_{70}, C_{76}, C_{78}, and C_{80}, and it was

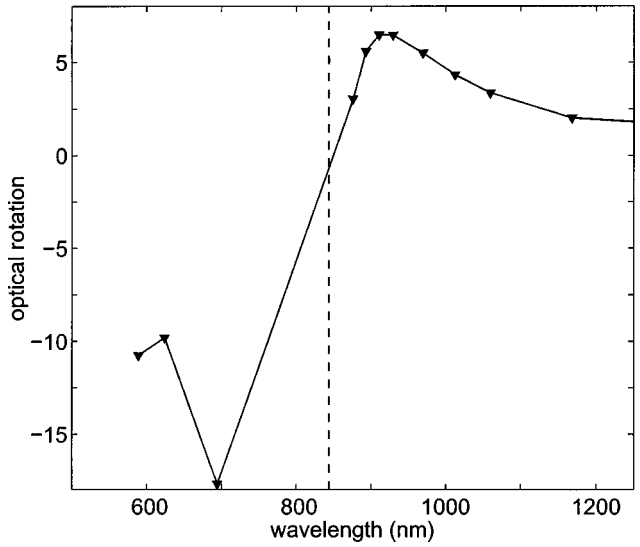

FIG. 4. Optical rotatory dispersion curve for the fullerene C_{84} obtained with TDKS/B3LYP. The vertical line mark the lowest singlet transition wavelength. The ORD is given in $10^{3\circ}/(\mathrm{dm\,g/cm^3})$ and the wavelength in nm.

concluded that TDKS theory allows for near-quantitative predictions of the dipole-allowed transitions.[33] Upon the application of a blueshift of 0.35 eV to all transition energies, spectral assignments could be made for the fullerenes studied.[33] For reasons of efficiency, the authors employed the nonhybrid BP86 functional, predicting the hybrid B3LYP exchange–correlation functional (used in the present work) to be superior. The experimental gap energy for the D_2 isomer of C_{80} in toluene solution is 1.43 eV, and there may be a solvent redshift of up to 500 cm^{-1} (0.06 eV).[33] With these things in mind, the experimental excitation energy for C_{80} compares favorably with our B3LYP lowest transition energy of 1.47 eV (corresponding to a wavelength of 844 nm) for the D_2 isomer of C_{84}. We conclude that we have a reasonably accurate description of the electronic structure of the ground and first excited states, which is crucial for an accurate dispersion of dynamic molecular properties.

The D_2 isomer of C_{84} is optically active but we are not aware of any experimental ORD measurements for this species. In the long-wavelength region, we predict a positive Cotton curve for the fullerene, see Fig. 4. The optical rotation is strong also in the non-resonant region, amounting to $2.00\times10^{3\circ}/(\mathrm{dm\,g/cm^3})$ at 1168 nm. At 910 nm, the ORD reaches a maximum—that is, its width is far larger than for 3MCH—and the use of damping becomes important about 150 nm from the first transition wavelength.

V. CONCLUSIONS

The complex linear polarization propagator has been extended to include mixed electric-dipole–magnetic-dipole properties with use of London atomic orbitals to ensure gauge-origin independent properties. Our implementation encompasses Hartree–Fock theory, multi-configurational self-consistent field theory, and Kohn–Sham DFT. Computational issues such as CPU cost and convergence of the iterative solutions of matrix equations are similar to those for the real propagator, as illustrated by the application of the complex propagator to the calculation of ORD to the fullerene C_{84} at the DFT/B3LYP level.

The technique presented in this work enables the treatment of ORD at frequencies in the nonresonant as well as resonant regions of the spectra. We have shown several examples of calculations of the anomalous dispersion that occurs in the resonant regions.

With careful tuning of the semiempirical damping parameter against experiment, it should be possible to use ORD measurements to estimate lifetimes of dipole-allowed excited states. We are also able to address the widths of the ORD spectra by theoretical calculations.

ACKNOWLEDGMENTS

This work has received support from Nordisk Forskerakademi (NorFA) which has made it possible for P.N. to visit Tromsø (Grant No. 020067). The National Supercomputer Centre (NSC) in Linköping, Sweden has provided the computer time needed for the fullerene calculations. The work has also received suppport from the Norwegian Research Council through a Strategic University Program in Quantum Chemistry (Grant No. 154011/420) and through a grant of computer time from the program for Supercomputing.

[1] C. Djerassi, *Optical Rotatory Dispersion: Applications to Organic Chemistry* (McGraw–Hill, New York, 1960).
[2] J. Olsen and P. Jørgensen, J. Chem. Phys. **82**, 3235 (1985).
[3] P. L. Polavarapu and C. Zhao, J. Am. Chem. Soc. **121**, 246 (1999).
[4] T. Helgaker, K. Ruud, K. L. Bak, P. Jørgensen, and J. Olsen, Faraday Discuss. **99**, 165 (1994).
[5] P. J. Stephens, F. J. Devlin, J. R. Cheeseman, and M. J. Frisch, J. Phys. Chem. A **105**, 5356 (2001).
[6] K. Ruud and T. Helgaker, Chem. Phys. Lett. **352**, 533 (2002).
[7] K. Ruud, P. J. Stephens, F. J. Devlin, P. R. Taylor, J. R. Cheeseman, and M. J. Frisch, Chem. Phys. Lett. **373**, 606 (2003).
[8] R. D. Amos, Chem. Phys. Lett. **87**, 23 (1982).
[9] F. London, J. Phys. Radium **8**, 397 (1937).
[10] J. Olsen, K. L. Bak, K. Ruud, T. Helgaker, and P. Jørgensen, Theor. Chim. Acta **90**, 421 (1995).
[11] H. S. French and M. J. Naps, J. Am. Chem. Soc. **58**, 2303 (1936).
[12] C. Djerassi and G. W. Krakower, J. Am. Chem. Soc. **581**, 237 (1959).
[13] P. Norman, D. M. Bishop, H. J. Aa. Jensen, and J. Oddershede, J. Chem. Phys. **115**, 10323 (2001).
[14] L. D. Barron, *Molecular Light Scattering and Optical Activity* (Cambridge University Press, Cambridge, 1982).
[15] A. D. Becke, J. Chem. Phys. **98**, 5648 (1994).
[16] P. L. Polavarapu, D. K. Chakraborty, and K. Ruud, Chem. Phys. Lett. **319**, 595 (2000).
[17] T. H. Dunning, Jr., J. Chem. Phys. **90**, 1007 (1989).
[18] D. E. Woon and T. H. Dunning, Jr., J. Chem. Phys. **100**, 2975 (1994).
[19] W. J. Hehre, R. Ditchfield, and J. A. Pople, J. Chem. Phys. **56**, 2257 (1972).
[20] S. Grimme, F. Furche, and R. Ahlrichs, Chem. Phys. Lett. **361**, 321 (2002).
[21] S. Grimme (private communication).
[22] A. Schäfer, H. Horn, and R. Ahlrichs, J. Chem. Phys. **97**, 2571 (1992).
[23] M. J. Frisch, G. W. Trucks, H. B. Schlegel *et al.*, GAUSSIAN 98 (1998). Gaussian Inc., Pittsburgh PA, 1998. See http://www.gaussian.com.
[24] T. Helgaker, H. J. Aa. Jensen, P. Jørgensen *et al.*, DALTON, an *ab initio* electronic structure program, Release 1.2. See http://www.kjemi.uio.no/software/dalton/dalton.html, 2001.
[25] S. Mukamel, *Principles of Nonlinear Optical Spectroscopy* (Oxford University Press, New York, 1995).
[26] M. Albota, D. Beljonne, J.-L. Brédas *et al.*, Science **281**, 1653 (1998).
[27] M. Pericou-Cayere, M. Rerat, and A. Dargelos, Chem. Phys. **226**, 297 (1998).

[28] K. Ruud, P. R. Taylor, and P.-O. Åstrand, Chem. Phys. Lett. **337**, 217 (2001).
[29] T. Müller, K. B. Wiberg, and P. H. Vaccaro, J. Phys. Chem. A **104**, 5959 (2000).
[30] E. Giorgio, C. Rosini, R. G. Viglione, and R. Zanasi, Chem. Phys. Lett. **376**, 452 (2003).
[31] P. J. Stephens, F. J. Devlin, J. R. Cheeseman, and M. J. Frisch, J. Phys. Chem. A **105**, 5356 (2001).
[32] J. A. Azamar-Barrios, T. J. S. Dennis, S. Sadhukan, H. Shinohara, G. E. Scusiera, and A. Pénicaud, J. Phys. Chem. A **105**, 4627 (2001).
[33] R. Bauernschmitt, R. Ahlrichs, F. H. Hennrich, and M. M. Kappes, J. Am. Chem. Soc. **120**, 5052 (1998).